Earth Syst. Dynam. Discuss., https://doi.org/10.5194/esd-2018-70
Manuscript under review for journal Earth Syst. Dynam.
Discussion started: 28 September 2018

Earth System Dynamics
Open Access
Discussions

An emergent transition time-scale in the atmosphere and its implications to global-averaged precipitation control mechanisms, time-series reconstruction and stochastic downscaling

Miguel Nogueira*
Instituto Dom Luiz, Faculdade de Ciências da Universidade de Lisboa
* corresponding author email: mdnogueira@fc.ul.pt

Abstract

Detrended Cross-Correlation Analysis (DCCA) revealed an emergent transition in non-periodic (deseasonalized) atmospheric variability at time-scales ~1-year. At multi-year time-scales (i) $\rho_{SST,Tland}$~0.6 (i.e. the correlation been global-averaged sea surface temperature, SST, and 2-meter air temperature averaged over global-land, T_{land}); (ii) Clausius-Clapeyron relationship becomes the dominant control of global-averaged precipitable water vapor (W), with $\rho_{W,T2m} \approx \rho_{W,SST}$~0.9; (iii) atmospheric radiative fluxes, specifically the surface downwelling longwave radiative flux (DLR), become a key constraint for global-mean precipitation (P) variability ($\rho_{P,Ratm} \approx \rho_{P,DLR}$~-0.8); (iv) cloud effects are negligible in (iii), and clear-sky DLR becomes a dominant P constraint; and (v) $\rho_{P,T2m}$ and $\rho_{P,SST}$ displayed significant multi-year correlations, although with large spread amongst different datasets (~0.4 to ~0.7). Result (v) provides a new perspective into the well-known uncertainties climate models associated with the dynamical component of precipitation. At sub-yearly time-scales all correlations underlying these five results decrease abruptly towards negligible values.

The relevance and validity of this multi-scale structure is demonstrated by three reconstructed P time-series at 2-year resolution, two relying on clear-sky DLR constraints and one based on P-SST correlation. These simple models, particularly one based on clear-sky DLR, were able to reproduce observed P anomaly time-series with similar accuracy to a (uncoupled) atmospheric model (ERA-20CM) and two climate reanalysis (ERA-20C and 20CR). The idealized models aren't applicable at sub-yearly time-scales, where the underlying correlations become negligible. However, monthly P probability density functions (PDFs) were derived by stochastic downscaling of reconstructed P,

Earth Syst. Dynam. Discuss., https://doi.org/10.5194/esd-2018-70
Manuscript under review for journal Earth Syst. Dynam.
Discussion started: 28 September 2018

leveraging on scale-invariant properties, outperforming the statistics simulated by ERA-20C, 20CR and ERA-20CM.

1. Introduction

The precipitation response to changes in increased concentrations of greenhouse gases is a central topic for the climate science community. Although its regional variability is essential to determine the societal impacts, global-averaged precipitation (P) is an important first-order climate indicator, and a measure of the global water cycle, that must be accurately simulated if robust climate projections are to be obtained across a wide range of spatial and temporal scales. However, even the long-term P response is still poorly understood, constrained and simulated (Collins et al., 2013; Allan et al., 2014; Hegerl et al., 2015), largely due to the limited knowledge on the complex interactions between the key components of the atmospheric branch of the water cycle and its forcing mechanisms. This problem is tackled here by employing a multi-scale analysis framework to study the variability of P, and its relation to two key governing mechanisms: the Clausius-Clapeyron (C-C) relationship and the constraints imposed by the atmospheric energy balance.

The C-C relationship is a well-known mechanism controlling the variability of the global water cycle. Assuming constant relative humidity, it implies that fractional changes in global-averaged precipitable water vapor ($\Delta W/W$) are linearly related to fluctuations of global-averaged near-surface (e.g. 2-meter) air temperature (ΔT_{2m}) (e.g. Held & Soden, 2006; Schneider et al., 2010):

$$\frac{\Delta W}{W} \approx \alpha_{W,T_{2m}} \Delta T_{2m}, \qquad (1)$$

where $\alpha_{W,T_{2m}} \approx 0.07$ K^{-1} at temperatures typical of the lower troposphere. Numerous studies have provided a robust confirmation for C-C at multi-decadal to centennial time-scales, while also reporting an analogous linear response of ΔP to ΔT (see e.g. Schneider et al., 2010; Trenberth, 2011; O'Gorman et al., 2012; and Allan et al., 2014 for reviews). In general, these previous investigations agree on the ~7%/K sensitivity coefficient for W. However, there is large spread on the P sensitivity coefficient estimates, typically in the 1%/K to 3%/K range.

A widely recognized explanation for the sub-C-C sensitivity of P to temperature fluctuations at long temporal scales comes from the atmospheric energy balance (Allen

Earth Syst. Dynam. Discuss., https://doi.org/10.5194/esd-2018-70
Manuscript under review for journal Earth Syst. Dynam.
Discussion started: 28 September 2018

& Ingram, 2002; Stephens & Ellis, 2008; Stephens & Hu, 2010). Specifically, averaging over the global atmosphere, the latent heat flux associated with precipitation formation (L_VP, L_V being the latent heat of vaporization) must be in balance with the net atmospheric radiative flux (R_{atm}) and the surface sensible flux (F_{SH}):

$$L_V P + R_{atm} + F_{SH} \approx 0, \quad (2)$$

Equation (2) represents a general state of radiative convective equilibrium (Pauluis & Held, 2002), with energy fluxes defined positive for atmospheric gain, and negative otherwise.

If the C-C relationship was the dominant mechanism controlling the response of atmospheric moisture content and the global water cycle to temperature fluctuations, then W and P could be expected to be strongly correlated to surface temperature. Previously Gu and Adler (2011, 2012) found strong correlations between the inter-annual variability of W and global-averaged surface temperature, in tight agreement with the C-C relationship. However, they found weaker (but significant) correlations between the inter-annual variability of P and global-averaged surface temperature, suggesting that C-C might not be directly extendable to global precipitation. But these results focusing on a single temporal scale might not represent the entire picture. In fact, it is now a well-established fact that precipitation and other relevant atmospheric variables (including temperature, atmospheric moisture, wind, etc.) display a complex statistical structure, with significant variability over a wide range of temporal scales, and with the possibility of different mechanisms governing variability at different time-scales (see e.g. Lovejoy & Schertzer, 2013 for a comprehensive review). Furthermore, it has been shown that this complex multiscale structure plays a role (at least) as important and the large amplitude periodic components, namely diurnal and seasonal cycles (Lovejoy, 2015; Nogueira, 2017a). However, our understanding of the underlying governing mechanisms at different time-scales remains largely elusive, representing a central problem for future improvements to climate simulation and projection.

Recently, Nogueira (2018) analyzed satellite-based observational datasets, a long Global Climate Model simulation and reanalysis products and found a tight correlation (~0.8) between anomaly (deseasonalized) time-series of W and global-averaged surface temperature, which emerged at time-scales larger than ~1-2 years. In contrast, at smaller time-scales the correlation decreased rapidly towards negligible values (<0.3). In other words, the C-C relationship is the dominant mechanism of deseasonalized W anomalies at multi-year time-scales, but not at sub-yearly time-scales. Nogueira (2018) also found

Earth Syst. Dynam. Discuss., https://doi.org/10.5194/esd-2018-70
Manuscript under review for journal Earth Syst. Dynam.
Discussion started: 28 September 2018

that the magnitude of the correlations between anomaly time-series for P and global-averaged surface temperature was negligible at sub-yearly time-scales, while at multi-year time-scales the results showed large spread amongst different data-sets, ranging between negligible (<0.3) and strong (~0.8) correlation values. Building on this previous study, here the multi-scale analysis of the mechanisms governing P variability is extended, including the energetic constraints on P represented in Equation (2). Additionally, a simple stochastic model is proposed to reconstruct P time-series based on the strong correlations found at multi-year time-scales, while monthly statistics are reproduced by employing a stochastic downscaling algorithm based on scale-invariant symmetries of P. The manuscript is organized as follows: section 2 describes the considered datasets and the multi-scale analysis framework; the results of multi-scale correlation analysis on P variability are presented and discussed in section 3; in section 4 a simple idealized model is proposed for reconstruction of P variability; and finally the main conclusions are summarized and discussed in section 5.

2. Data and Methodology

2.1. Data sets

Observations of P were obtained from the Global Precipitation Climatology Project (GPCP) version 2.3 monthly precipitation dataset (Adler et al., 2003), which covers the full globe at 2.5º resolution from 1979 to present. Gridded datasets of monthly average surface temperatures were obtained from the Goddard Institute for Space Studies (GISSTEMP) analysis (Hansen et al., 2010), which covers the globe at 2º resolution from 1880 to present, with the values provided as anomalies relative to the 1951-1980 reference period. GISSTEMP blends near-surface air temperature measurements from meteorological stations (including Antarctic stations) with a reconstructed SST dataset over oceans. Observations of atmospheric radiative fluxes were obtained from the National Aeronautics and Space Administration (NASA) Clouds and the Earth's Radiant Energy System, Energy Balanced and Filled (CERES-EBAF) Edition 4.0 (Loeb et al., 2009), a monthly dataset covering the full globe at 1º resolution from March/2000 to June/2017.

Two state-of-the-art reanalyses of the twentieth-century were considered in the present study. One was the National Oceanic and Atmospheric Administration Cooperative institute for Research in Environmental Sciences (NOAA-CIRES) twentieth-century reanalysis (20CR) version 2c (Compo et al., 2011), which covers the full globe at 2º resolution, spanning from 1851 to 2014. Only surface pressure observations and reports are assimilated in this reanalysis. SST boundary conditions are obtained from 18 members of pentad Simple Ocean Data Assimilation with Sparse Input (SODAsi) version 2, with the high latitudes corrected to the Centennial in Situ Observation-Based Estimates of the Variability of SST and Marine Meteorological Variables, version 2 (COBE-SST2). Here, global-mean time-series of P, W, SST, T_{2m}, DLR and OLR are obtained from 20CR at daily resolution for the 1900-2010 period. R_{atm} cannot be obtained the incoming solar radiation at TOA is not available for the 20CR dataset, due to an error with output processing.

The other reanalysis considered in the present study was the European Centre for Medium-Range Weather Forecasts (ECMWF) twentieth-century reanalysis (ERA-20C, Poli et al., 2015), which covers the full globe at 1º resolution spanning from 1900-2010. It assimilates marine surface winds from the International Comprehensive Ocean-Atmosphere Data Set version 2.5.1 (ICOADSv2.5.1) and surface and mean-sea-level pressure from the International Surface Pressure Databank version 3.2.6 (ISPDv3.2.6) and from ICOADSv2.5.1. SST boundary conditions are obtained from the Hadley Centre Sea Ice and Sea Surface Temperature data set version 2.1 (HadISST2.1). Global-mean time-series of P, W, SST, T_{2m}, R_{atm}, DLR and OLR are obtained from ERA-20C at daily resolution for the 1900-2010 period.

Finally, the uncoupled ECMWF twentieth-century ensemble of ten atmospheric model integrations (ERA-20CM, Hersbach et al., 2015) was considered, which uses the same model, grid, initial conditions, radiative and aerosol forcings as ERA-20C. However, no observations are assimilated, the simulation is integrated continuously over the full 1900-2010 period, and SST is prescribed by an ensemble of realizations from HadISST2.1, including one control simulation and nine simulations with perturbed SST and sea-ice concentration. A 10-member ensemble of global-mean time-series of P, W, SST, T_{2m}, R_{atm}, DLR and OLR were obtained from ERA-20CM at monthly resolution for the 1900-2010 period. Considering ERA-20CM allowed to test the sensitivity of the multi-scale correlation structure derived from ERA-20C to data assimilation, but different atmospheric evolutions associated with perturbations to the forcing fields (particularly to SST).

Notice that the clear-sky radiative fluxes considered here obtained from ECMWF datasets are computed for the same atmospheric conditions of temperature, humidity, ozone, trace gases and aerosol, but assuming that the clouds are not there. Clear-sky estimates from

Earth Syst. Dynam. Discuss., https://doi.org/10.5194/esd-2018-70
Manuscript under review for journal Earth Syst. Dynam.
Discussion started: 28 September 2018

Earth System Dynamics
Discussions
Open Access

ERA-20C and ERA-20CM cover the full globe area and not just the cloud free regions at each time instant. However, they are available for net radiative fluxes, but not for downwelling or upwelling radiation fluxes.

2.2. Detrended Cross-Correlation Analysis (DCCA)

DCCA allows to accurately quantify power-law correlations between two different time-series over wide ranges of time-scales (Podobnik & Stanley, 2008). Consider two time-series, y and y', with N data points each. Due to the strong yearly cycle present in the considered time-series, the periodic seasonal trend is first eliminated by subtracting the long-term average (over all the years in the record) of each calendar day (or month, depending on temporal resolution):

$$\Delta y(i) = y(i) - \langle y \rangle_d, \tag{3}$$

Then two integrated signals, R and R', are constructed from the deseasonalized anomaly time-series, Δy and $\Delta y'$:

$$R_k = \sum_{i=1}^{k}[\Delta y(i) - \langle y_{ds} \rangle], \tag{4}$$

Where k=1,…,N and ⟨ ⟩ indicates temporal averaging. The integrated signals are divided into $N-n$ overlapping segments, each containing $n+1$ values. For each segment from each integrated signal, the "local trend" is estimated using a first-order polynomial. The detrended integrated signal is then defined as the difference between the original integrated signal and the local trend $(R_v - \widetilde{R_v})$, where $\widetilde{R_v}$ is the fitting first-order polynomial to the vth segment R_v. Next, the covariance of the residuals in each segment is calculated as:

$$f_{R,R'}{}^2(n,i) = \frac{1}{n+1}\sum_{k=i}^{i+n}\left[(R_v - \widetilde{R_v})(R_v{}' - \widetilde{R_v{}'})\right], \tag{5}$$

The detrended covariance is estimated by summing over all overlapping N-n segments:

$$F^2_{R,R'}(n) = \frac{1}{N-n}\sum_{i=1}^{N-n} f^2_{R,R'}(n,i), \tag{6}$$

Finally, the DCCA cross-correlation coefficient at time-scale n, $\rho_{y,y'}(n)$, is defined as the ratio between the detrended covariance function and the product of the square-rooted detrended variance function for each time-series:

$$\rho_{y,y'}(n) = \frac{F^2_{R,R'}(n)}{\sqrt{F^2_{R,R}(n) \times \sqrt{F^2_{R',R'}(n)}}}, \tag{7}$$

The values of $\rho_{y,y'}(n)$ range between -1 and 1 (for perfect negatively and positively correlated signals, respectively). It has been previously shown that critical points for the 95% significance level of $|\rho_{DCCA}|$ can vary between values below 0.1 and up to about 0.4, depending on the time series length, the considered time-scale, and the power law exponents of both time-series (Podobnik et al., 2011). Here it is assumed that $|\rho_{DCCA}|$ values below 0.3 are nonsignificant, and that $|\rho_{DCCA}|$ values in the 0.3 to 0.4 range should be interpreted with care.

3. DCCA analysis of the mechanisms governing P variability across time-scales

3.1. Multi-scale structure of the atmospheric water cycle response to surface temperature fluctuations

DCCA reveals strong correlations (~0.9) between deseasonalized anomaly time-series for W and T_{2m} or SST at multi-year time-scales (Fig. 1a). However, as the time-scale decreases there is a transition in the correlation structure, and negligible correlations (<0.3) emerge at sub-yearly time-scales. This result suggested that the C-C relationship in Equation (1) holds to a very good approximation at multi-year time-scales, but not at sub-yearly time-scales. Lovejoy et al. (2018) employed multi-scale analysis framework based on Haar wavelets to GISSTEMP and found a similar transition in the multi-scale correlation structure of SST against global-averaged surface temperature, between low-correlations at time-scales below a few months and strong correlations (~0.8) at multi-year time-scales. These strong correlations weren't surprising, since SST was a major component in their definition of global-averaged surface temperature (also considering SST over the ocean pixels and 2-meter air temperature over land pixels). But their results also showed a transition in the correlation coefficients between SST and near-surface air temperature over global-land (T_{land}), with maximum correlation values ~0.6 at multi-year time-scales. The transition in $\rho_{SST,Tland}$ was confirmed here by employing DCCA to ERA-20C, ERA-20CM, 20CR and GISSTEMP (Fig. 1b). Thus, the present results support Lovejoy et al. (2018) argument that these abrupt correlation changes correspond to a fundamental behavioral transition, where the atmosphere and the oceans start to act as a single coupled system. Furthermore, the results presented here suggest that W anomalies at multi-year resolution can be derived, to a very good approximation, from SST alone.

Nogueira (2018) also reported a transition in the multi-scale correlation structure between deseasonalized anomaly time-series of P and global-averaged surface temperature (considering SST over the oceans and T_{2m} over land), with negligible values at sub-yearly time-scales, but with large spread in the magnitude of the multi-year correlations, ranging

Earth Syst. Dynam. Discuss., https://doi.org/10.5194/esd-2018-70
Manuscript under review for journal Earth Syst. Dynam.
Discussion started: 28 September 2018

between values ~0.3 to ~0.8. Here, a similar result was found for $\rho_{P,T_{2m}}$ and $\rho_{P,SST}$ (Fig. 1c), with large spread in correlation magnitude at multi-year time-scales (~0.7 in ERA-20C and ERA-20CM, ~0.6 in 20CR, and <0.4 in observations). This large spread and the relatively low correlations obtained from observational datasets confirmed the uncertainty on the extension of C-C relationship as the dominant control of P variability. Notice that the large spread in $\rho_{P,T2m}$ and $\rho_{P,SST}$ represents a different perspective, under a multi-scale analysis framework, on a previously established fact: there are large uncertainties in climate simulations associated with the role of the non-thermodynamical (circulation) component of precipitation response to climate change (see e.g. Shepherd, 2014).

3.2. Multi-scales structure of the energetic constraints to P variability

A study of the circulation component of the P response to temperature fluctuations requires a detailed representation of several spatially heterogeneous variables and their nonlinear interactions. An alternative path towards understanding P variability was taken in the present investigation, focusing on the constraints imposed by the atmospheric energy balance represented in Equation (2). Fig. 2a (solid lines) shows that the estimated DCCA correlation coefficients between the deseasonalized anomaly time-series for P and R_{atm} were strongly (negatively) correlated at multi-year time-scales ($\rho_{P,R_{atm}} \sim -0.8$ in ERA-20C, ERA-20CM and observations), in agreement with the balance in Equation (2). The same wasn't true at sub-yearly time-scales, where the correlation magnitude decreased rapidly, changed sign around monthly time-scales, and reached values ~0.4 at time-scales below about 10 days.

Considering the effect of F_{SH} in Equation (2) (i.e. $\rho_{P,R_{atm+F_{SH}}}$) slightly increased the (positive) correlations at sub-monthly time-scales (Fig. 2a, dashed lines), although the absolute changes are essentially below 0.1 and $\rho_{P,R_{atm+F_{SH}}}$ at sub-monthly time-scales (which is only available for the ERA-20C dataset). More importantly, the change between $\rho_{P,R_{atm}}$ and $\rho_{P,R_{atm+F_{SH}}}$ at multi-year time-scales was negligible. Indeed, $\rho_{P,R_{F_{SH}}}$ displayed values up to about 0.5 at sub-monthly time-scales, but essentially <0.4 at multi-year time-scales (Fig. 2a, dot-dashed lines). Given the results in Fig. 1a, the following linear relation was hypothesized: $L_V \Delta P \approx c_1 \times (-\Delta R_{atm}) + c_2$, where c_1 and c_2 are arbitrary constants, and Δ represents fluctuations taken as deseasonalized anomalies at multi-year resolutions. At sub-yearly time-scales this simplification is not

Earth Syst. Dynam. Discuss., https://doi.org/10.5194/esd-2018-70
Manuscript under review for journal Earth Syst. Dynam.
Discussion started: 28 September 2018

adequate, since $\rho_{P,R_{atm}}$ becomes negligible and, thus, the energy balance represented in Equation (2) doesn't represent the dominant constraint on P variability, most likely due to non-negligible changes in atmospheric heat storage.

The analysis was extended by decomposing R_{atm} into its net atmospheric longwave and shortwave radiative flux components, i.e. $R_{atm} = R_{LW,net} + R_{SW,net}$. On the one hand, $\rho_{P,R_{atm}} \approx \rho_{P,R_{LW,net}}$ over the full range of time-scales considered (Fig. 2b). On the other hand, $\rho_{P,R_{SW,net}}$ also displays significant values (~0.6) at multi-year time-scales, but the latter magnitude was nearly 0.2 lower than $\rho_{P,R_{atm}}$ and $\rho_{P,R_{LW,net}}$ (Fig. 2b). Consequently, the above linear relationship for multi-scale P anomalies was further refined as $L_V \Delta P \approx c_1 \times (-\Delta R_{atm}) + c_2 \approx c_3 \times (-\Delta R_{LW,net}) + c_4$, where c_3 and c_4 are arbitrary constants. Subsequently, $R_{LW,net}$ was further decomposed into the top-of-atmosphere (TOA) and surface net longwave fluxes, i.e. $R_{LW,net} = R_{LW,TOA} + R_{LW,SFC}$. At multi-year time-scales, $\rho_{P,R_{atm}} \approx \rho_{P,R_{LW,SFC}}$ (Fig. 2c). $\rho_{P,R_{LW,TOA}}$ also displayed significant values at multi-year time-scales, up to ~-0.6 in ERA-20C and ERA-20CM datasets. Notice that 20CR displayed values $|\rho_{P,R_{LW,TOA}}| < 0.4$ at multi-year time-scales. But ECMWF datasets were in better agreement with observations, suggesting that significant (negative) correlations existed between P and $R_{LW,TOA}$ anomalies at multi-year time-scales. Nonetheless, even for ECMWF and observational products, the magnitude of $\rho_{P,R_{LW,TOA}}$ at multi-year time-scales was nearly 0.2 lower than for $\rho_{P,R_{LW,SFC}}$. Consequently, a further approximation was considered on the linear model for P fluctuations at multi-year time-scales: $L_V \Delta P \approx c_1 \times (-\Delta R_{atm}) + c_2 \approx c_3 \times (-\Delta R_{LW,net}) + c_4 \approx c_5 \times (-\Delta R_{LW,SFC}) + c_6$.

Finally, $R_{LW,SFC}$ can be further decomposed into its upwelling ($R_{LW,SFC,UP}$) and downwelling ($R_{LW,SFC,DOWN}$, henceforth denoted downwelling longwave radiation, DLR) components. Fig. 2d shows that, at multi-year time-scales, the differences between $\rho_{P,R_{DLR}}$ and $\rho_{P,R_{atm}}$ were within 0.1 in observations, ERA-20C and ERA-20CM (R_{atm} is unavailable for 20CR). Thus, at multi-year time-scales, the fluctuations in downwelling surface longwave radiative fluxes are, to a good approximation, linearly related to P fluctuations: $L_V \Delta P \approx c_7 \times (-\Delta DLR) + c_8$. Notice that the differences between $\rho_{P,R_{LW,SFC,UP}}$ and $\rho_{P,R_{atm}}$ are identically low in observations, but these differences are somewhat higher (~0.2) in ERA-20CM and ERA-20C. Thus, a similar linear relationship between ΔP and $\Delta R_{LW,SFC,UP}$ might also hold to a good approximation, although the correlations are less robust than for ΔP against ΔDLR.

The correlation between global-mean clear-sky net radiative atmospheric heating and P, i.e. $\rho_{P,R_{atm,cs}}$, was nearly identical to $\rho_{P,R_{atm}}$ at multi-year time-scales (Fig. 3a). This suggested that the cloud effects on the multi-year linear dependence between P variability and net atmospheric radiative fluxes may be neglected. But the same isn't true at time-scales below a few months, where significant differences emerge between $\rho_{P,R_{atm,cs}}$ and $\rho_{P,R_{atm}}$. This clear-sky approximation holds at multi-year time-scales for correlations of P against global-averaged net atmospheric longwave radiative fluxes and, also, and against the global-averaged net surface longwave fluxes (Fig. 3b). Based on these results, it was further hypothesized that cloud effects are also negligible for the correlation between P and DLR at multi-year temporal scales. This hypothesis could not be tested directly because clear-sky DLR time-series were not available for the ECMWF datasets. Nonetheless, the results in Section 4 based on an empirical algorithm for DLR estimation under a clear-sky approximation provided support for this hypothesis.

In summary, DCCA suggested that P variability at multi-year time-scales is linearly related to the net atmospheric radiative fluxes. Furthermore, this linear relationship is dominated by its longwave component and, more specifically, by the surface longwave radiative fluxes, particularly DLR. DCCA also suggests that clouds play a negligible effect in these linear correlations at multi-years scales. The hypothesized tight correlation between P and clear-sky DLR fluxes at multi-year time-scales was particularly interesting, since clear-sky DLR may be estimated directly from atmospheric water vapor content and surface temperature (e.g. Stephens et al., 2012b). This fact will be further explored below, in Section 4.

Finally, notice that the results in Fig. 2c showed that P variability was best correlated to $R_{LW,TOA}$ variability at sub-monthly time-scales, reaching positive values ~0.5-0.6. This corresponds to a well-known relation between convective rainfall and the outgoing longwave radiation at TOA, often denoted OLR (e.g. Xie & Arkin, 1998). However, this result provided no further simplification in the sense that, unlike for clear-sky DLR at multi-year resolution, it is equally difficult to model and predict P and OLR (including cloud effects) at sub-monthly time-scales.

At this point, it is important to notice that the existence of strong correlations does not necessarily imply causality between two variables. However, the atmospheric energy

Earth Syst. Dynam. Discuss., https://doi.org/10.5194/esd-2018-70
Manuscript under review for journal Earth Syst. Dynam.
Discussion started: 28 September 2018

balance in Equation (2) provides a physical basis for the obtained strong (negative) correlations values between P and atmospheric radiative fluxes. In fact, the importance of energetic constraints to global precipitation, the dominant role of surface longwave fluxes, namely DLR, and the negligible cloud effects in these relations has been pointed out by previous investigations (e.g., Stephens and Hu, 2010; Stephens et al., 2012a,b). The DCCA presented here provided further robustness to these results. More importantly, a clear transition emerged between robust correlations at multi-year time-scales and negligible correlations at sub-yearly time-scales, which was found for P against R_{atm} (or DLR), for W against T_{2m} (and SST), for SST against T_{land} and, less robustly, for P against T_{2m} (or SST). Given the interdependence between these variables, these transitions are likely to be interrelated, representing a more fundamental transition in the atmosphere. Notice that these results also contribute to sharpen the picture from previous studies reporting a 'fast' P response at sub-monthly time-scales, where P is suggested respond directly to the radiative effects of increasing CO_2; and a 'slow' response where P increases due to increasing surface temperature (Allen & Ingram, 2002; Bala et al., 2010; Andrews et al., 2010; O'Gorman et al., 2012; Allan et al., 2014).

4. Stochastic model for global-mean precipitation

4.1. Reconstruction of P time-series at multi-year resolution

Here a very simple model for P response to climate change is proposed aiming to demonstrate the robustness of the tight correlation between P and clear-sky DLR (DLR_{CS}) at multi-year time-scales presented in Section 3. The rationale is that the correlation between P and DLR_{CS} at multi-year time-scales is significantly more robust than between P and T_{2m} (or SST). Additionally, DLR_{CS} can be derived, to a good approximation, from the global averaged near-surface temperature alone (e.g. Stephens et al., 2012b). Furthermore, given the tight coupling between T_{land} and SST at multi-year time-scales (Fig. 1b), it is hypothesized that DLR_{CS} variability could be obtained, to a good approximation directly from the SST forcing. This hypothesis is also supported by the nearly identical correlations between W and T_{2m} or SST (Fig. 1a).

Here two different algorithms to estimate DLR_{CS} are tested: the Dilley-O'Brien model (Dilley & O'Brien, 1998), and the Prata model (Prata, 1996). In the Dilley-O'Brien model:

$$DLR_{2y,DO} = a_1 + a_2\left(\frac{SST_{2y}}{SST_c}\right)^6 + a_3\left(\frac{\Delta W_{2y}+W_c}{W_c}\right)^{1/2}, \quad (8)$$

Earth Syst. Dynam. Discuss., https://doi.org/10.5194/esd-2018-70
Manuscript under review for journal Earth Syst. Dynam.
Discussion started: 28 September 2018

Earth System Dynamics
Discussions

Where a_1 = 59.38 Wm^{-2}, a_2 = 113.7 Wm^{-2} and a_3 = 96.96 Wm^{-2} are the model parameters, and $W_c = 22.5$ kg m^{-2} is the climatological value for W. The subscript '2y' (e.g. DLR_{2y}) indicates a time-series at 2-year resolution. The fluctuations Δ represent anomaly time-series relative to a climatological time-series, for example $\Delta DLR_{2y,DO} = DLR_{2y,DO} - DLR_{c,DO}$. Notice that for multi-year resolution time-series, this yields the same result as first deseasonalizing the time-series (using Equation (3)) and then coarse-graining it to 2-year resolution. $DLR_{c,DO} = a_1 + a_2 + a_3$ is obtained by replacing the climatological values of W and SST in Equation (8).

The Prata model for $\Delta DLR_{2y,Pr}$ is based on the Stefan-Boltzmann equation:

$$DLR_{2y,Pr} = \varepsilon_{clr}\sigma_{SB}{SST_{2y}}^4 \tag{9}$$

Where $\sigma_{SB} = 5.67 \times 10^{-8}$ Wm^{-2}K^{-4} is the Stefan-Boltzmann constant and:

$$\varepsilon_{clr} = 1 - \left(1 + W_{2y}\right)\exp(-\left(1.2 + 3W_{2y}\right)^{1/2}) \tag{10}$$

The anomaly-time series is computed from $\Delta DLR_{2y,Pr} = DLR_{2y,Pr} - DLR_{c,Pr}$, where $DLR_{c,Pr}$ is obtained by replacing the climatological values of W and SST in Equations (9) and (10).

The high values of $\rho_{W,SST} (\approx \rho_{W,T_{2m}})$ at multi-year time-scales (Section 3.1) allowed to remove the W dependence in Equations (8) and (11), by replacing $W_{2y} \approx \alpha_{W,SST}\Delta SST_{2y}W_c + W_c$. The forcing ΔSST_{2y} time-series were obtained by coarse-graining the deseasonalized (using Equation (3)) global-averaged SST obtained from GISSTEMP dataset. The sensitivity coefficient, $\alpha_{W,SST} \approx 0.08\ K^{-1}$ was estimated by least-square regression of $\Delta W_{2y}/W_c$ against ΔSST_{2y}, pooling together all datasets (ERA-20C, ERA-20CM and 20CR). The $\alpha_{W,SST}$ estimates are summarized in Table 1, including for each individual dataset, ranging between 0.07 and 0.10 K^{-1}. Notice that the obtained values are close to the typical 0.07 K^{-1} value.

The results from Section 3.2 suggested a linear relation between P and DLR_{CS} variability at multi-year time-scales, which can be written as $P_{2y} \approx \alpha_{P,DLR}(-\Delta DLR_{CS,2y})P_c + P_c$. In this way, two reconstructed anomaly time-series for P were obtained, $P_{2y,DO}$ and $P_{2y,Pr}$, respectively by replacing $\Delta DLR_{CS,2y}$ with $\Delta DLR_{2y,DO}$ and $\Delta DLR_{2y,Pr}$. The coefficient $P_c \approx 2.7$ mm/day was estimated from GPCP dataset. The sensitivity coefficient $\alpha_{P,DLR} \approx$ 0.004 (W/m^2)$^{-1}$ was estimated by least-square regression of $\Delta P_{2y}/P_c$ against ΔDLR_{2y}, pooling together all available datasets (ERA-20C, ERA-20CM, 20CR and GPCP against CERES-EBAF). Notice that, in estimating $\alpha_{P,DLR}$, clear-sky DLR time-series were used

Earth Syst. Dynam. Discuss., https://doi.org/10.5194/esd-2018-70
Manuscript under review for journal Earth Syst. Dynam.
Discussion started: 28 September 2018

where available (i.e. for ERA-20C and ERA-20CM) datasets, but they were replaced by (full-sky) DLR otherwise (i.e. for 20CR and CERES-EBAF). The $\alpha_{P,DLR}$ estimates are summarized in Table 2, including values obtained from each dataset (no estimate was made for GPCP against CERES-EBAF due to the limited duration of the latter), ranging between 0.003 $(W/m^2)^{-1}$ and 0.005 $(W/m^2)^{-1}$.

Another simple linear model for reconstruction of multi-year P anomaly time-series was tested, based on the direct response (correlations) of P to SST fluctuations, i.e. $P_{2y,SST} \approx \alpha_{P,SST}\Delta SST_{2y}P_c + P_c$. Again, the ΔSST_{2y} was obtained from GISSTEMP dataset. The sensitivity coefficient, $\alpha_{P,SST} \approx 0.02\ K^{-1}$ was estimated by least-square regression of $\Delta P_{2y}/P_c$ against ΔSST_{2y}, pooling together all datasets (ERA-20C, ERA-20CM, 20CR and GPCP against GISSTEMP). The $\alpha_{P,SST}$ estimates are summarized in Table 3, including for each individual dataset, ranging between 0.02 and 0.04 K^{-1}. Notice that the obtained values are close to the 0.01 to 0.03 K^{-1} range reported in the relevant literature (e.g. Schneider et al., 2010; Trenberth, 2011; O'Gorman et al., 2012; and Allan et al., 2014).

When compared against ΔP_{2y} directly derived from GPCP for the 1979 to 2010 period, the errors in the proposed linear ΔP_{2y} reconstructions were generally close to those for atmospheric model-based products (Fig. 4). $\Delta P_{2y,Pr}$ displays the highest mean bias, somewhat higher than for atmospheric model-based datasets, but also higher than the mean bias for $\Delta P_{2y,DO}$ and $\Delta P_{2y,SST}$ (Fig. 4a). Notice that all atmospheric model-based products considered here also display a positive bias. While this may be due a negative bias of GPCP (e.g. Gehne et al., 2015), this observational dataset represents the longest reliable dataset for global precipitation studies and thus was considered here as 'the truth'. More importantly, the mean bias is easy to correct, simply by subtracting its value from the time-series. This correction was implemented here for all atmospheric model-based and linear-model based ΔP_{2y} time-series. Figure 4c shows that the normalized standard deviation ($\sigma_n = \sigma_{2y,model}/\sigma_{2y,obs}$) estimated from $\Delta P_{2y,DO}$ (~0.4) and, particularly, from $\Delta P_{2y,SST}$ (~0.3) were lower than the values estimated from atmospheric model-based products (~0.5-0.9). In contrast, σ_n estimated from $\Delta P_{2y,Pr}$ was nearly 0.8, which was higher than 20CR and most members in the ERA-20CM ensemble, only outperformed by ERA-20C dataset. The root-mean squared error after bias-correction ($RMSE_{bc}$) estimated from $\Delta P_{2y,Pr}$ and $\Delta P_{2y,DO}$ were well within the range of the values obtained from atmospheric model-based products (Fig. 4b), with the Prata model slightly

Earth Syst. Dynam. Discuss., https://doi.org/10.5194/esd-2018-70
Manuscript under review for journal Earth Syst. Dynam.
Discussion started: 28 September 2018

overperforming the Dilley-O'Brien model. $RMSE_{bc}$ estimated from $\Delta P_{2y,SST}$ was on the high-end of the atmospheric model-based range of values, and somewhat worse than for the DLR-based linear models. Finally, the Pearson correlation coefficient between models and observations (Fig. 4d) was similar amongst all linear-based models and well within the range of values estimated from the atmospheric model-based products. The latter result was expected since all linear models were forced by the same SST time-series.

Overall, these results suggested that $\Delta P_{2y,Pr}$ (after bias correction) reproduced the observations with similar accuracy to atmospheric model-based products, including similar $RMSE_{bc}$, variability amplitude and phase of the signal. $\Delta P_{2y,DO}$ displayed similar performance for $RMSE_{bc}$ and for the phase, but not for the variability amplitude. Finally, $\Delta P_{2y,SST}$ had the worst performance concerning $RMSE_{bc}$, but also in capturing the variability amplitude, while it displayed similar ability to the other linear models in reproducing the phase. The overall weakest performance of $\Delta P_{2y,SST}$ was coherent with the less robust correlations underlying this model. Additionally, the results indicate that the non-linear transformations on SST employed in the Prata and the Dilley-O'Brien algorithms improved the linear models.

4.2. Stochastic reproducing of P monthly PDFs

At sub-yearly time-scales, the magnitude of $\rho_{P,W}$, $\rho_{P,SST}$ and $\rho_{P,DLR}$ decreased abruptly to negligible values (Section 3). Thus, at these time-scales, the C-C relationship is no longer the dominant control of W (nor P) variability, and the longwave radiative fluxes are no longer the main constraints for P. Additionally, the cloud-effects on P variability become non-negligible (Fig. 3). Consequently, the linear relationships underlying the above P reconstruction at 2-year resolution are no longer appropriate at sub-yearly time-scales. Building on the strong scale-invariant symmetries present in the variability of global and regional rainfall across wide ranges of time-scales (e.g. Lovejoy and Schertzer, 2013; Nogueira et al., 2013; Nogueira and Barros, 2014, 2015; Nogueira, 2017, 2018), an algorithm was proposed here to derive the sub-yearly statistics from the multi-year information alone. The physical basis for this algorithm is that while the atmosphere is governed by continuum mechanics and thermodynamics, it simultaneously obeys statistical turbulence cascade laws (e.g., Lovejoy & Schertzer, 2013; Lovejoy et al., 2018).

Conveniently, precipitation (and many other atmospheric variables) is characterized by low spectral slopes $\beta < 1$, with quasi-Gaussian and quasi-non-intermittent statistics, at time-scales between ~10 days and a few decades (Lovejoy & Schertzer, 2013; de Lima & Lovejoy, 2015; Lovejoy et al., 2015, 2018; Nogueira, 2017b, 2018). Grounded by these scale-invariant properties, fractional Gaussian noise was used here to generate multiple realizations of downscaled ΔP at monthly resolution from each member of each ΔP_{2y} time-series:

$$\Delta P_{1m}(t) = fGn_{1m}(t)\frac{\Delta P_{2y}(t)}{fGn_{2y}(t)} \quad (11)$$

where fGn_{1m} is a fractional Gaussian noise, which was computed by first generating a random Gaussian noise (g), then taking its Fourier transform ($\tilde{g}$), multiplying by $k^{-\beta/2}$, and finally taking the inverse transform to obtain fGn_{1m}. The mean of fGn_{1m} was forced to be equal to the number of data-points of ΔP_{2y}. Then fGn_{2y} was obtained by coarse-graining fGn_{1m} using 24-point (i.e. 2 years) length boxes. In this way, $\Delta P_{1m,DO}$, $\Delta P_{1m,Pr}$, $\Delta P_{1m,SST}$ ensembles are generated respectively from the bias-corrected $\Delta P_{2y,DO}$, $\Delta P_{2y,Pr}$ and $\Delta P_{2y,SST}$ time-series. One hundred plausible realizations are generated for each ensemble, corresponding to one hundred different realizations of fGn_{1m}. Based on recent investigations on P scale-invariance properties, a spectral exponent $\beta \approx 0.3$ is assumed (de Lima & Lovejoy, 2015; Nogueira, 2018). In Equation (11), the 2-year resolution time-series were assumed to have a constant value for every month inside each 2-years period. Notice that a resolution limit should exist to the proposed stochastic downscaling algorithm, namely at time-scales below ~10 days where a fundamental transition occurs in the scaling behavior of most atmospheric fields (including P, see e.g. Lovejoy & Schertzer, 2013; Lovejoy, 2015; de Lima & Lovejoy, 2015; Nogueira, 2017a,b, 2018). At faster time-scales intermittency becomes non-negligible and the quasi-Gaussian approximation to the statistics is no longer robust.

The proposed downscaling methodology corresponds to treating the sub-yearly frequencies as random 'weather noise', which is characterized, to a good approximation, by scale-invariant behavior with quasi-Gaussian statistics (Vallis, 2009; Lovejoy et al., 2015). A similar downscaling methodology has been previously demonstrated to reproduce the spatial sub-grid scale variability of topographic height (Bindlish & Barros, 1996), rainfall (Bindlish & Barros, 2000; Rebora et al., 2006; Nogueira & Barros, 2015) and clouds (Nogueira & Barros, 2014).

Figure 5a showed that the PDFs computed from $\Delta P_{1m,DO}$, $\Delta P_{1m,Pr}$ and $\Delta P_{1m,SST}$ were in remarkable agreement with GPCP PDFs for the 1979-2010 period, representing a significant improvement compared to all atmospheric model-based products. This improved PDF accuracy was quantified using the Perkins skill score, S-Score (Perkins et al., 2007), defined as:

$$\text{S-Score}=100 \times \sum_{i=1}^{M} min[f_{mod}(i), f_{obs}(i)] \tag{12}$$

where $f_{mod}(i)$ and $f_{obs}(i)$ are respectively the frequency of the modeled and observed P anomaly values in bin i, M is the number of bins used to compute the PDF (here M=15), and min[x,y] is the minimum between the two values. The S-Score is a measure of similarity between modeled and observed PDFs, such that if a model reproduces the observed PDF perfectly then S-Score=100%.

The linear-based models showed S-Score values around 95%, which were significantly higher than then ~80% found for the atmospheric model-based products (Fig. 6). Furthermore, the stochastic model captured the change in the PDFs between two separate periods (1979-1990 and 1999-2010, Fig. 5b), while preserving the remarkably high (≥90%) S-Scores (Fig. 6, blue and red markers). Indeed, the S-Scores for linear-based were consistently better than the S-Scores obtained from atmospheric model-based products (~80%). Despite some differences between PDFs obtained from $\Delta P_{1m,DO}$, $\Delta P_{1m,Pr}$ and $\Delta P_{1m,SST}$, their similar performance in reproducing observations was somewhat unexpected, given the distinct performances in reproducing the observed time-series at multi-year resolutions. While the error analysis here was based on a limited sample (mainly due to short duration of the satellite-period), these results suggested that the proposed stochastic downscaling mechanism is quite robust in reproducing the monthly P statistics, with only moderate sensitivity to the coarse resolution forcing.

5. Conclusions

Atmospheric variables display significant variability over a wide range of temporal scales, both due changes in external forcings (including surface fluxes, changes to greenhouse gases and aerosol concentrations, solar forcing, and volcanic eruptions), but also due to intrinsic modes of atmospheric variability. Additionally, external and internal atmospheric processes interact nonlinearly amongst themselves, resulting in an intricate multi-scale structure, which is still ill understood and responsible for significant uncertainties in climate models. Here a multi-scale analysis framework was employed, aiming to disentangle the complex structure of global-averaged precipitation variability.

A critical transition emerges from DCCA at time-scales ~1-year, revealing a change in the control mechanisms of the P and W, but also in the strength of the atmosphere-ocean coupling. At multi-year time-scales W becomes tightly correlated to T_{2m} and to SST (~0.9), while at sub-yearly time-scales this correlation decreases abruptly towards negligible values (~0.2). A sensitivity coefficient for W close to the typically estimated 0.07%/K was found for multi-year time-scales. In other words, the C-C relationship is the dominant mechanism of W at multi-year time-scale, but not at sub-year time-scales. Furthermore, at time-scales >1-2 years SST becomes tightly correlated to T_{land}, pointing to a fundamental behavioral transition, where the atmosphere and the oceans start to act as a single coupled system at multi-year time-scales, as previously suggested by Lovejoy et al. (2018).

A similar transition was also found for $\rho_{P,T_{2m}}$ and $\rho_{P,SST}$, with negligible correlations and sub-year time-scales, which tend increase at multi-year time-scales, although the latter displayed significant spread amongst different datasets (ranging between ~0.4 to ~0.7).

More robust correlations were obtained for the P response to the energetic constraints imposed by a simple atmospheric energy balance. DCCA showed that P variability is tightly (negatively) coupled to the net atmospheric radiative balance at multi-year time-scales (with $\rho_{P,R_{atm}} \lesssim -0.8$). The transition between multi-year and sub-yearly time-scales also emerged for $\rho_{P,R_{atm}}$, with the correlation magnitude decreased rapidly at sub-yearly time-scales, changing signal, and reached values ~0.4 at sub-monthly time-scales. Additionally, DCCA revealed that the positive sub-monthly correlations are dominated by the TOA OLR, while the multi-year correlations were dominated by surface longwave fluxes, particularly by DLR. Furthermore, DCCA suggested that cloud effects play a negligible on the multi-year correlations, but they are important for the sub-monthly $\rho_{P,R_{atm}}$ values. Notice that the sensitivity coefficients of P to SST estimated here were in the 2-4%/K range, close to the typical 1-3%/K values (for P against T_S) obtained from energetic constraints on global rainfall.

The robustness and relevance of this emergent multi-scale correlation structure is demonstrated by proposing simple models for reconstruction of P at multi-year time-scales. Anomaly time-series for P at 2-year resolution were derived from SST observations alone, either directly based on $\rho_{P,SST}$, or by combining $\rho_{R,DLR_{CS}}$, empirical algorithms for clear-sky DLR estimation, and the C-C relationship. After correcting for their systematic mean bias, the highly-idealized model for ΔP_{2y} based on clear-sky DLR estimated from the Prata algorithm displayed similar accuracy in reproducing observations as atmospheric model-based products, as measured by $RMSE_{bc}$, Pearson

Earth Syst. Dynam. Discuss., https://doi.org/10.5194/esd-2018-70
Manuscript under review for journal Earth Syst. Dynam.
Discussion started: 28 September 2018

Earth System Dynamics
Open Access
Discussions

correlation coefficient and normalized standard deviation. The simple model based on the Dilley-O'Brien algorithm for clear-sky DLR estimation showed a somewhat poorer performance, particularly in reproducing the observed variability amplitude. Finally, the model based on P-SST correlation showed the weakest performance, which agrees with the less robust correlations underlying this idealized model.

The proposed linear models cannot be extended to sub-yearly the time-scales because all the correlations upon which they rely become negligible. This abrupt transition in the multi-scale correlation structure implies that at sub-yearly time-scales the tight linear coupling between atmospheric and ocean temperature, the Clausius-Clapeyron relationship, and the atmospheric energy balance are no longer dominant linear constraints for P. Nonetheless, the multi-scale analysis framework provides another path for reconstruction of the P statistics at sub-yearly resolution. A stochastic downscaling algorithm based on scale-invariant symmetries of P was applied to ΔP_{2y} reconstructed time-series, resulting in monthly P PDFs. Remarkably, the reconstructed PDFs of P at monthly resolution showed better accuracy in reproducing GPCP statistics than atmospheric model-based products, as measured by S-Score computed over decadal and 30-year periods. Interestingly, the PDFs obtained by downscaling the three algorithms proposed for multi-year P reconstruction showed similar performance, suggesting a weak sensitivity of this algorithm to the accuracy of the 2-year resolution forcing time-series.

The present investigation highlights the complex multi-scale structure of the water cycle variability and its governing mechanisms. Finally, it is hypothesized that the path for stochastic regional precipitation simulation may be opened by leveraging on the widely reported scale-invariant properties of precipitation in the spatial domain (e.g. Lovejoy a& Schertzer, 2013; Nogueira & Barros, 2014, 2015), and exploring control mechanisms for slow variability of regional precipitation, such as the El-Niño Southern Oscillation and its teleconnections.

Acknowledgements

This study was funded by the Portuguese Science Foundation (F.C.T.), under grant UID/GEO/50019/2013, as part of research project SOLAR (PTDC/GEOMET/7078/2014).

ERA-20C and ERA-20CM were provided by ECMWF and are available through the website http://apps.ecmwf.int/datasets.

Earth Syst. Dynam. Discuss., https://doi.org/10.5194/esd-2018-70
Manuscript under review for journal Earth Syst. Dynam.
Discussion started: 28 September 2018

20CR reanalysis, GISSTEMP and GPCP precipitation product were provided by the NOAA/OAR/ESRL PD, Boulder, Colorado, USA, from their website http://www.esrl.noaa.gov/psd.
The CERES-EBAF data were obtained from the NASA Langley Research Center Atmospheric Science Data Center, from their website https://eosweb.larc.nasa.gov/project/ceres/ebaf_surface_table

References

Adler, R. F., Huffman, G. J., Chang, A., Ferraro, R., Xie, P.-P., Janowiak, J., Rudolf, B., Schneider, U., Curtis, S., Bolvin, D., Gruber, A., Susskind, J., Arkin, P., and Nelkin, E.: The Version-2 Global Precipitation Climatology Project (GPCP) monthly precipitation analysis (1979–Present), J. Hydrometeorol., 4(6), 1147–1167, doi:10.1175/1525-7541(2003)004<1147:TVGPCP>2.0.CO;2, 2003.

Allan, R. P., Liu, C., Zhan, M., Lavers, D. A., Koukouvagias, E., and Bodas-Salcedo, A.: Physically consistent responses of the global atmospheric hydrological cycle in models and observations. Surv. Geophys. **35**, 533-552, 2014.

Allen, M.R., and Ingram, W. J.: Constraints on future changes in climate and the hydrologic cycle. Nature **419**, 224-232, 2002.

Andrews, T., Forster, P. M., Boucher, O., Bellouin, N., and Jones, A.: Precipitation, radiative forcing and global temperature change. Geophys. Res. Lett. **37**, L14701, 2010.

Bala, G., Caldeira, K., and Nemani, R.: Fast versus slow response in climate change: Implications for the global hydrological cycle. Clim. Dyn. **35**, 423-434, 2010.

Bindlish, R., and Barros, A. P.: Aggregation of digital terrain data using a modified fractal interpolation scheme. Comput. Geosci. (UK) **22**, 907-917, 1996.

Bindlish, R., & Barros, A. P.: Disaggregation of rainfall for one-way coupling of atmospheric and hydrological models in regions of complex terrain. Global Planet. Chang, **25(12)**, 111-132, 2000.

Collins, M., Knutti, R., Arblaster, J., Dufresne, J.-L., Fichefet, T., Friedlingstein, P., Gao, X., Gutowski, W. J., Johns, T., Krinner, G., Shongwe, M., Tebaldi, C., Weaver, A. J., and Wehneret, M.: Long-term climate change: Projections, commitments and

Earth Syst. Dynam. Discuss., https://doi.org/10.5194/esd-2018-70
Manuscript under review for journal Earth Syst. Dynam.
Discussion started: 28 September 2018

irreversibility, in Climate Change 2013: The Physical Science Basis. Contribution of Working Group I to the Fifth Assessment Report of the Intergovernmental Panel on Climate Change, edited by T. F. Stocker et al., pp. 1029–1136, Cambridge Univ. Press, Cambridge, U. K., and New York, 2013.

Compo, G. P., Whitaker, J. S., Sardeshmukh, P. D., Matsui, N., Allan, R. J., Yie, X., Gleason, B. E., Vose, R. S., Rutledge, G., Bessemoulin, P., Brönimann, S., Brunet, M., Crouthamel, R. I., Grant, A. N., Groisman, P. Y., Jones, P. D., Kruk, M. C., Kruger, A. C., Marshall, G. J.,Maugeri, M., Mok, H. Y., Nordli, O., Ross, T. F., Trigo, R. M., Wang, X. L., Woodruff, S. D., and Worley, S. J.: The Twentieth Century Reanalysis Project. Q. J. R. Meteorol. Soc. **137**, 1-28, 2011.

Dilley, A. C., and O'Brien, D.M.: Estimating downward clear-sky long-wave irradiance at the surface from scree temperature and precipitable water. Q. J. R. Meteorol. Soc. **124A**, 1391-1401, 1998.

Gehne, M., Hamill, T. M., Kiladis, G. N., and Trenberth, K. E.: Comparison of Global Precipitation Estimates across a Range of Temporal and Spatial Scales. J. Clim. **29**, 7773-7795, 2016.

Gu G, and Adler R. F.: Precipitation and temperature variations on the interannual time scale: assessing the impact of ENSO and volcanic eruptions. J Clim 24:2258–2270, 2011.

Gu, G. and Adler, R. F.: Large-scale, inter-annual relations among surface temperature, water vapour and precipitation with and without ENSO and volcano forcings. Int. J. Climatol., 32: 1782–1791. doi:10.1002/joc.2393, 2012.

Hansen, J., R. Ruedy, M. Sato, and Lo, K.: Global surface temperature change, Rev. Geophys., 48, RG4004, doi:10.1029/2010RG000345, 2010.

Hegerl, G. C., Black, E., Allan, R. P., Ingram, W. J., Polson, D., Trenberth, K., Chadwick, R. S., Arkin, P. A., Sarojini, B. B., Becker, A., Dai, A., Durack, P. J., Easterling, D., Fowler, H. J., Kendon, E. J., Huffman, G. J., Lu, C., Marsh, R., New, M., Osborn, T. J., Skliris, N., Stott, P. A., Vidale, P.-L., Wijffels, S. E., Wilcox, L. J., Willet, K. M., and Zhang, X.: Challenges in quantifying changes in the global water cycle. Bull. Am. Meteorol. Soc. **96**, 1097–1115, 2015.

Held, I. M. and Soden, B. J.: Robust responses of the hydrological cycle to global warming. J. Clim. **19**, 5686-5699, 2006.

Hersbach, H., Peubey, C., Simmons, A., Berrisford, P., Poli, P. and Dee, D. P.: ERA-20CM: A twentieth century atmospheric model ensemble. Q. J. R. Meteorol. Soc. **141**, 2350-2375, 2015.

de Lima, M. I. P. and Lovejoy, S.: Macroweather precipitation variability up to global and centennial scales. Water. Resour. Res. **51**, 9490-9513, 2015.

Loeb, N. G., Wielicki, B. A., Doeling, D. R., Smith, G. L., Keyes, D. F., Kato, S., Manalo-Smith, N., and Wong, T.: Toward Optimal Closure of the Earth's Top-of-Atmosphere Radiation Budget. J. Clim. **22**, 748-766, 2009.

Lovejoy S, and Schertzer, D.: The Weather and Climate: Emergent Laws and Multifractal Cascades, Cambridge University Press, Cambridge, 2013.

Lovejoy, S.: A voyage through scales, a missing quadrillion and why the climate is not what you expect, Clim. Dynam., 44, 3187–3210, 2015.

Lovejoy, S., del Rio Amador, L. and Hébert, R.: The ScaLIng Macroweather Model (SLIMM): Using scaling to forecast global-scale macroweather from months to decades. Earth System Dynamics **6**, 1-22, 2015.

Lovejoy, S., Del Rio Amador, L., and Hébert, R.: Harnessing butterflies: theory and practice of the Stochastic Seasonal to Interannual Prediction System (StocSIPS), in Tsonis A. (eds) Advances in Nonlinear Geosciencs, Springer, Cham, 2018.

Nogueira, M., and Barros, A. P.: The nonconvective/convective structural transition in stochastic scaling of atmospheric fields. J. Geophys. Res. Atmos. **119**, 771-794, 2014.

Nogueira, M., & Barros, A. P.: Transient stochastic downscaling of quantitative precipitation estimates for hydrological applications. J.Hydrol. **529(3)**, 1407-1421, 2015.

Nogueira, M.: Exploring the link between multiscale entropy and fractal scaling behavior in near-surface wind. PLoS ONE 12(3): e0173994. https://doi.org/10.1371/journal.pone.0173994, 2017a.

Nogueira, M.: Exploring the links in monthly to decadal variability of the atmospheric water balance over the wettest regions in ERA-20C. J. Geophys. Res.: Atmos. **122**,560–577, 2017b.

Nogueira, M.:The sensitivity of the atmospheric branch of the global water cycle to temperature fluctuations at synoptic to decadal time-scales in different satellite- and model-based products. Clim. Dyn. https://doi.org/10.1007/s00382-018-4153-z, 2018.

O'Gorman, P. A., Allan, R. P., Byrne, M. P. and Previdi, M.: Energetic constraints on precipitation under climate change. Surv. Geophys. **33**, 585-608, 2012.

Pauluis, O., & Held, I.: Entropy budget of an atmosphere in radiative-convective equilibrium. Part I: Maximum work and frictional dissipation, J. Atmos. Sci., 59, 125-139, https://doi.org/10.1175/1520-0469(2002)059<0125:EBOAAI>2.0.CO;2, 2002.

Perkins, S., Pitman, A., Holbrook, N. and McAneney, J.: Evaluation of the AR4 Climate Models' Simulated Daily Maximum Temperature, Minimum Temperature, and Precipitation over Australia Using Probability Density Functions. J. Clim. **20**, 4356-4376, 2007.

Podobnik, B., and Stanley, H. E.: Detrended Cross-Correlation Analysis: A New Method for Analyzing Two Nonstationary Time-Series. Phys. Rev. Lett. **100**, 084102, 2008.

Podobnik, B., Jiang, Z., Zhou, W. & Stanley, H. E.: Statistical tests for power-law cross-correlated processes. Phys. Rev. E **84**, 06618, 2011.

Poli, P., Hersbach, H., Dee, D. P., Berrisford, P., Simmons, A. J., Vitart, F., Laloyaux, P., Tan, D., Peubey, C., Thépaut, N., Trémolet, Y., Hólm, E. V., Bonavita, M., Isaksen, L., and Fisher, M.: ERA-20C: An Atmospheric Reanalysis for the Twentieth Century. J. Clim. **29**, 4083-4097, 2015.

Prata, A. J.: A new long-wave formula for estimating downward clear-sky radiation at the surface. Q. J. R. Meteor. Soc. **122**, 1127-1151, 1996.

Rebora, N., Ferraris, L., von Hardenberger, J., and Provenzale, A.: RainFARM: Rainfall downscaling by a filtered autoregressive model, J. Hydrometerol., 7, 724-738, 2006.

Schneider, T., O'Gorman, P. A. and Levine, X. J.: Water vapor and the dynamics of climate changes. Rev. Geophys. **48**, RG3001, 2010.

Shepherd, T. G.: Atmospheric circulation as a source of uncertainty in climate change projections. Nat. Geosci. **7**, 703–708, 2014.

Earth Syst. Dynam. Discuss., https://doi.org/10.5194/esd-2018-70
Manuscript under review for journal Earth Syst. Dynam.
Discussion started: 28 September 2018

Stephens, G. L. and Ellis, T. D.: Controls of global-mean precipitation increases in global warming GCM experiments. J. Clim. **21**, 6141-6155, 2008.

Stephens, G. L., and Hu, Y.: Are climate-related changes to the character of global precipitation predictable? Environ. Res. Lett. **5**, 025209, 2010.

Stephens, G. L., Li, J., Wild, M., Clayson, C. A., Loeb, N., Kato, S., L'Ecuyer, T., Stackhouse Jr., P. W., Lebsock, M., and Andrews, T.: An update on Earth's energy balance in light of the latest global observations. Nat. Geosci. **5**, 691-696, 2012a.

Stephens, G. L., Wild, M., Stackhouse Jr., P. W., L'Ecuyer, T., Kato, S., and Henderson, D. S.: The global character of the flux of downward longwave radiation. J. Clim. **25**, 557-571, 2012b.

Trenberth, K. E.: Changes in precipitation with climate change, Clim. Res., 47, 123–138, 2011.

Vallis, G. K.: Mechanisms of climate variability from years to decades. In Palmer, T. N.., & Williams, P. (eds.) Stochastic Physics and Climate Modelling, 1-34, Cambridge University Press, Cambridge, 2009.

Xie, P., and Arkin, P. A.: Global Monthly Precipitation Estimates from Satellite-Observed Outgoing Longwave Radiation, J. Climate, 11, 137-164. https://doi.org/10.1175/1520-0442(1998)011<0137:GMPEFS<2.0.CO;2, 1998.

Earth Syst. Dynam. Discuss., https://doi.org/10.5194/esd-2018-70
Manuscript under review for journal Earth Syst. Dynam.
Discussion started: 28 September 2018

Table 1 Linear regression coefficient $\alpha_{W,SST}$ estimated from ΔW/W$_c$ against ΔSST at 2-year resolution, assuming a relationship as given by Equation (1). The respective coefficient of determination is also provided. The $\alpha_{W,SST}$ are computed for ERA-20C, 20CR, and for the ensemble of ERA-20CM simulations. Additionally, the coefficient is estimated by pooling together ERA-20C, ERA-20CM (ensemble) and 20CR datasets.

Dataset	$\alpha_{W,SST}$ $[K^{-1}]$	R^2
ERA-20C	0.09	0.97
20CR	0.10	0.92
E20CM (Ensemble)	0.07	0.92
All Datasets	0.08	0.91

Table 2. Linear regression coefficient $\alpha_{P,DLR}$ estimated from ΔP/P$_c$ against ΔDLR at 2-year resolution, assuming a relationship as given by Equation (11). The respective coefficients of determination are also provided. The $\alpha_{P,DLR}$ values are computed for ERA-20C, 20CR, and for the ensemble of ERA-20CM simulations. Additionally, the coefficient is estimated by pooling together all datasets, including GPCP observations against DLR from CERES-EBAF.

Dataset	$\alpha_{P,DLR}$ $[(Wm^{-2})^{-1}]$	R^2
ERA-20C	0.005	0.88
20CR	0.003	0.51
E20CM (Ensemble)	0.004	0.81
All datasets (includes observations)	0.004	0.70

Table 3. Linear regression coefficient $\alpha_{P,SST}$ estimated from ΔP/P$_c$ against ΔSST at 2-year resolution. The respective coefficients of determination are also provided. The $\alpha_{P,SST}$ values are computed for ERA-20C, 20CR, for the ensemble of ERA-20CM simulations, and for GPCP against ERA-20CM control SST forcing. Additionally, the coefficient is estimated by pooling together all datasets.

Dataset	$\alpha_{P,SST}$ $[K^{-1}]$	R^2
ERA-20C	0.04	0.89
20CR	0.02	0.35
E20CM (Ensemble)	0.02	0.73
GPCP	0.04	0.42
All datasets (includes observations)	0.02	0.53

Earth Syst. Dynam. Discuss., https://doi.org/10.5194/esd-2018-70
Manuscript under review for journal Earth Syst. Dynam.
Discussion started: 28 September 2018

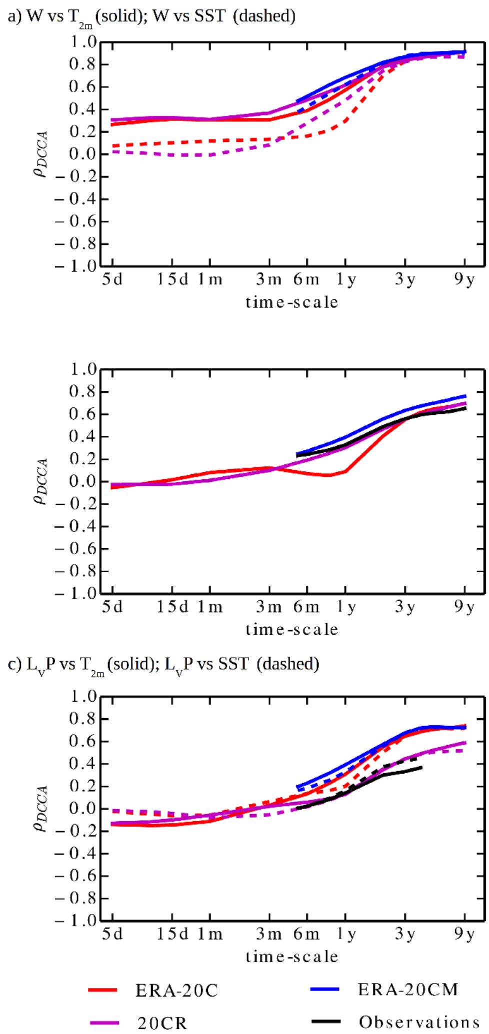

Figure 1. DCCA cross-correlation coefficients against temporal scale computed for global-mean time-series of a) W vs T_{2m} (solid) and W vs SST (dashed); b) SST vs T_{land}; and c) L_vP vs T_{2m} (solid) and L_vP vs SST (dashed). Red lines represent results from ERA-20C, blue lines are from ERA-20CM, pink lines are from 20CR and black lines are estimated from observational products. Notice that R_{atm} is not available from 20CR dataset, and that observational-based estimates of ρ_{P,T_S} (and $\rho_{P,SST}$) are only computed up to 4-year time-scales due to the limited duration of GPCP dataset.

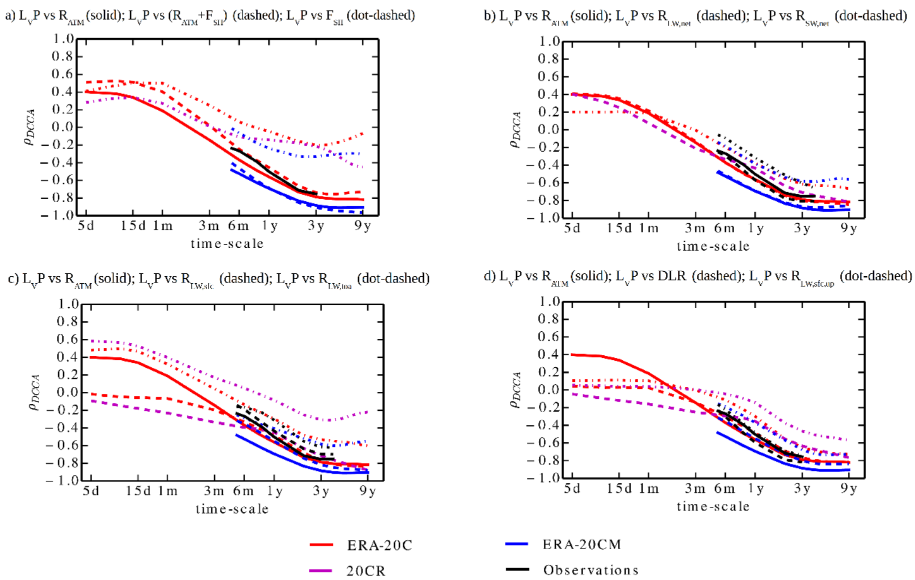

Figure 2. DCCA cross-correlation coefficients against temporal scale computed for a) L_vP vs R_{atm} (solid), L_vP vs ($R_{atm} + F_{SH}$) (dashed) and L_vP vs F_{SH} (dot-dashed); b) L_vP vs R_{atm} (solid), L_vP vs $R_{LW,net}$ (dashed), and L_vP vs $R_{SW,net}$ (dot-dashed); c) L_vP vs R_{atm} (solid), L_vP vs $R_{LW,SFC}$ (dashed), and L_vP vs $R_{LW,TOA}$ (dot-dashed); and d) L_vP vs R_{atm} (solid), L_vP vs DLR (dashed), and L_vP vs $R_{LW,SFC,UP}$ (dot-dashed). Red lines are computed from ERA-20C, blue lines are from ERA-20CM, pink lines are from 20CR and black lines are computed from GPCP and CERES-EBAF observational products. Notice that R_{atm} and $R_{SW,net}$ are not available from 20CR, and that correlation coefficients estimated from observational products are only computed up to 4-year time-scales due to the limited duration of GPCP dataset.

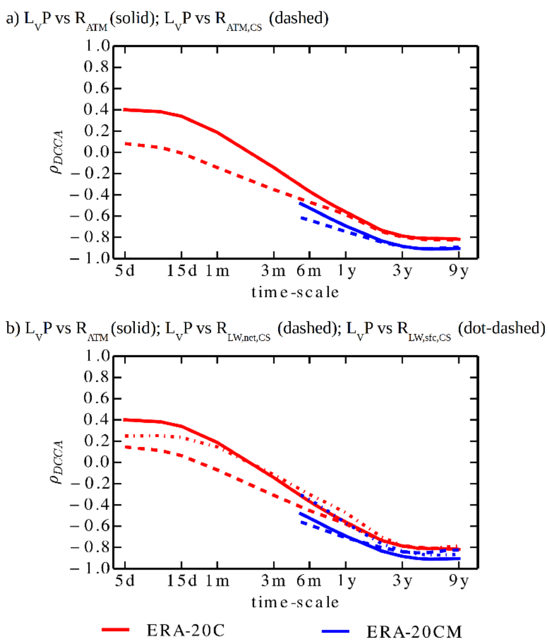

Figure 3. DCCA cross-correlation coefficients against temporal scale computed for a) L_vP vs R_{atm} (solid) and L_vP vs $R_{atm,CS}$ (dashed); b) L_vP vs $R_{LW,SFC}$ (solid) and L_vP vs $R_{LW,SFC,CS}$ (dashed). Red lines are computed from ERA-20C and blue lines are from ERA-20CM.

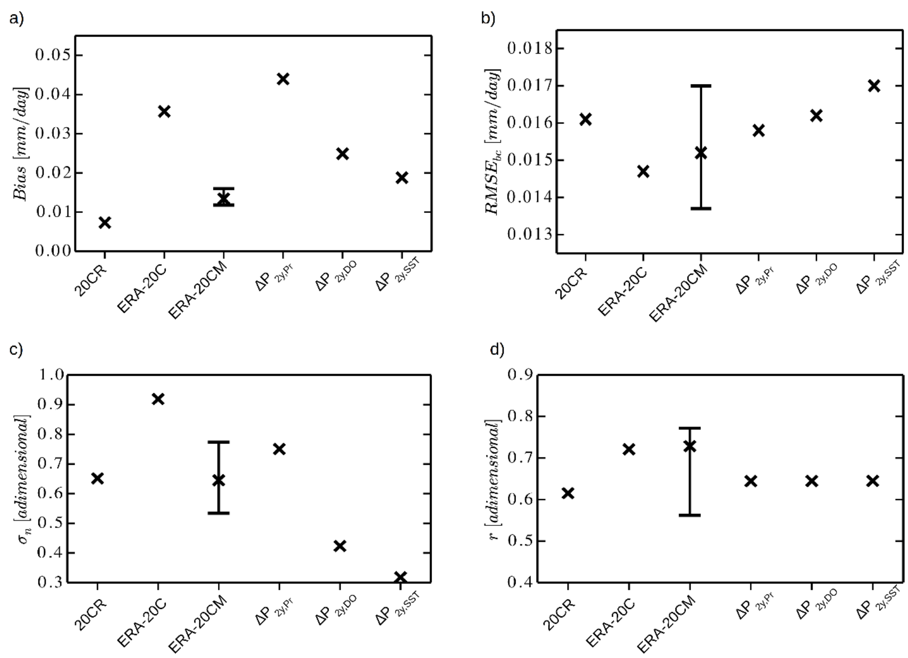

Figure 4. Error estimates from simulated anomaly time-series for P at 2-year resolution against GPCP, computed for the 1979-2010 period, including a) mean bias (Bias); b) root-mean-square error after bias correction ($RMSE_{bc}$); c) model standard deviation normalized by observed standard deviation (σ_n); and d) Pearson correlation coefficient (r). For ERA-20CM dataset the range for all ensemble members is shown, while 'x' marks their mean value. The p-value for all correlations shown in panel (d) are <0.05.

Earth Syst. Dynam. Discuss., https://doi.org/10.5194/esd-2018-70
Manuscript under review for journal Earth Syst. Dynam.
Discussion started: 28 September 2018

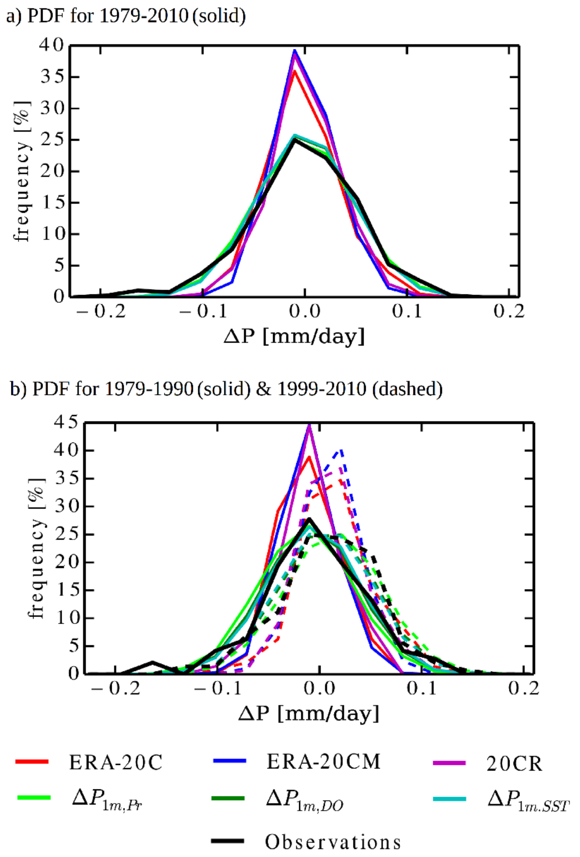

Figure 5. PDFs estimated from monthly anomaly time-series for P from ERA-20C (red), ERA-20CM (dark blue), 20CR (pink), GPCP (black), $\Delta P_{1m,DO}$ (dark green), $\Delta P_{1m,Pr}$ (light green), and $\Delta P_{1m,SST}$ (light blue). In panel a) the PDFs are estimated for the 1979-2010 period, and in panel b) the PDFs are estimated for the 1979-1990 period (solid) and the 1999-2010 period (dashed).

Earth Syst. Dynam. Discuss., https://doi.org/10.5194/esd-2018-70
Manuscript under review for journal Earth Syst. Dynam.
Discussion started: 28 September 2018

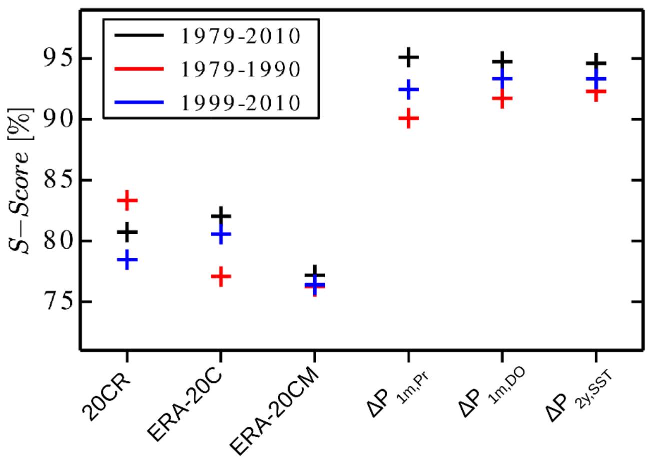

Figure 6. S-Score computed from the different P simulations against GPCP. The values estimated for the full satellite period (1979-2010) are presented in black, for the 1979-1990 period are presented in red, and for 1990-2010 period are presented in blue. For ERA-20CM dataset, the S-Score is estimated from the 10-member ensemble PDF.